

Vibrational Spectra of Lumazine in Water at pH 2–13: Ab Initio Calculation and FTIR/Raman Spectra

Craig Hemann,[†] Predrag Ilich,[‡] and Russ Hille^{*,†}

Department of Molecular and Cellular Biochemistry, The Ohio State University, Columbus, Ohio 43210, and The Department of Chemistry & Biochemistry, Loras College, Dubuque, Iowa 52004

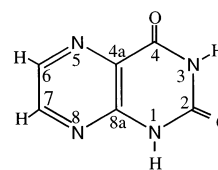
Received: June 12, 2002

Harmonic vibrational frequencies and transition intensities of lumazine (2,4-(1H,3H)pteridinedione in the neutral state) have been calculated in a self-consistent reaction field of high dielectric medium ($\epsilon = 78.54$) using ab initio Hartree–Fock (HF) and hybrid HF/density functional theory (DFT) methods. For the DFT method, the 4-31G basis set and the three parameter exchange functional of Becke combined with the Lee, Yang, and Parr correlational functional are used. The 6-31+G* basis set is used in the HF calculations. Both the spherical cavity model (SCM) and the self-consistent isodensity polarizable continuum model (SCIPCM) are used to simulate an aqueous environment for the N-protonated lumazines. For the N-deuterated lumazines, only the SCM is used. Simple scaling of the vibrational frequencies resulting from the DFT calculations incorporating the reaction field models of neutral lumazine, lumazine A1/N3-H monoanion, and lumazine A1,A3-dianion compare closely with Raman and Fourier transform infrared spectra of lumazine taken in aqueous media (both H₂O and D₂O) over a wide pH/pD range. The mean deviation between calculated and experimental vibrational frequencies is 9.10 cm⁻¹ for neutral lumazine (9.37 cm⁻¹ in D₂O), 9.18 cm⁻¹ for the monoanion (10.77 cm⁻¹ in D₂O), and 16.06 cm⁻¹ for the dianion (16.00 cm⁻¹ when prepared in D₂O). Calculated vibrational energy shifts with changes in ionization exhibit many trends that are evident in the experimental data although the absolute magnitudes of many of the individual shifts do not agree exactly. The calculated H/D isotopic shifts for the neutral and monoanionic species of lumazine agree well with those seen experimentally. Correlating shifts with ionization and the H/D isotopic shifts of the vibrational modes of each species of lumazine investigated have resulted in normal mode assignments of all in-plane vibrational modes observed in the 300–1750 cm⁻¹ range in aqueous solution.

Introduction

Lumazine (2,4-(1H,3H)pteridinedione) (I, Chart 1) is a naturally occurring pteridine derivative known to function as substrate in the oxidative hydroxylation reaction catalyzed by xanthine oxidase resulting in the product violapterin (2,4,7-(1H,3H,8H)pteridinetrione). It also possesses the pyrimidine and pyrazine subnuclei common with the ubiquitous isalloxazine ring of flavin cofactors. Steady state and kinetic studies of the reaction of xanthine oxidase with lumazine have demonstrated that a long wavelength species forms with a maximum absorbance at 650 nm that represents a charge transfer complex between the reduced molybdenum center of the enzyme and the product violapterin.^{1–3} This species can also be formed by addition of violapterin to enzyme reduced by sodium dithionite and has been shown to be stable as long as an anaerobic condition is maintained. In a resonance Raman study, Oertling et al. have used 677 nm excitation to selectively enhance the Raman active vibrational modes due to this Mo(IV)/violapterin complex.^{4–6} An empirical analysis of the Raman spectra concluded that the majority of the resonance-enhanced vibrations was due to internal vibrations of the coordinated violapterin, although certain oxygen isotope sensitive shifts were assigned to the Mo(IV)–O–R linkage of the complexed violapterin. A

CHART 1: (I) Neutral Lumazine-2,4(1H,3H)pteridinedione



more detailed interpretation of the feature-rich spectra was limited by the lack of vibrational assignments for either violapterin or lumazine. This lack of information has prompted us to explore ab initio methods to aid in making such assignments.

Our theoretical study is based on careful mapping of midinfrared spectroscopic properties of aza-aromatic cofactors in aqueous media over a wide range of pH values. In the preceding study, we performed ab initio Gaussian calculations of fundamental harmonic vibrations of uracil (in its pyrimidine dione form) using different basis sets (for example, Pople's 4-31G and 6-31+G), different methods of calculations (HF and DFT), and different versions of simulated continuous environment (Kirkwood–Onsager^{14–17} and IPCM^{18–20}). After we carried out the harmonic vibrational calculations for each uracil protonation form separately (cation, neutral, two anion forms, and dianion), we modeled the vibrational spectra in aqueous media at selected pH values by combining the calculated vibrational parameters, energies and transition strengths, in

* To whom correspondence should be addressed. Tel: 614 292-3545. E-mail: hille.1@osu.edu.

[†] The Ohio State University.

[‡] Loras College.

proportion to the pK_a values of the respective protonation forms. In this way, we obtained theoretical spectra of uracil in water and D_2O , over the pH/pD range of 0.7–13, in fair agreement with FTIR and Raman experiments.⁷

In the present study, we have applied the same type of analysis to the pteridine derivative, lumazine. Full molecular geometry optimizations and vibrational calculations using both the DFT-B3LYP and the HF methods incorporating the Kirkwood–Onsager SCM and the SCIPCM demonstrate that neutral lumazine, lumazine A1/N3H-monoanion, and lumazine A1,A3-dianion (A1 refers to deprotonation at the N1 position and A3 refers to deprotonation at the N3 position) are the most probable tautomeric forms for each ionization state in aqueous medium over the pH/pD 2.2–13.0 range. Raman and infrared spectra are simulated for both the N-protonated and N-deuterated forms of each of these lumazine species, and vibrational mode correlations are made between neutral lumazine, the A1/N3H-monoanion, and the A1,A3-dianion. Many of the predicted frequency shifts due to a change in protonation state of lumazine are apparent in the experimental spectra. It is also possible to correlate vibrational mode H/D isotopic shifts for the N-protonated and N-deuterated forms of neutral lumazine as well as the lumazine A1/N3H-monoanion. The predicted H/D isotopic shifts for each of these species agree well with experiment and, combined with mode correlations of ionic forms of lumazine, have permitted unambiguous normal mode assignments.

In our previous study of uracil, it was possible to include a detailed analysis of the effects of solvation on several protonation states of uracil using vibrational analyses of uracil in argon matrix and crystalline forms found in the literature (ref 7 and references therein). This type of analysis was not undertaken in this work due to the lack of vibrational data of this type for the lumazine molecule in the literature. For our purposes, it was more important to perform all analyses on lumazine in aqueous solvent.

Materials and Methods

Experiment. Lumazine was purchased from Aldrich (97% pure) and further purified by the method of Albert et al.²¹ D_2O (99.9% enriched), DCl (20% w/w in D_2O), and NaOD (38.9% w/w in D_2O) were purchased from Cambridge Isotope Laboratories. Samples were prepared unbuffered with pH/pD adjustments made by adding minute amounts of either H(D)Cl or NaOH(D). All pD values reported were obtained by adding 0.4 to the pH meter readings.²²

Infrared spectra were collected on a Mattson Sirius 100 FTIR interferometer at 1.0 cm^{-1} resolution. Each data set consisted of signal-averaging 4096 double-sided interferograms. Triangular apodization of the interferogram was performed using the real part of the Fourier transform to generate a single-beam spectrum. Each sample or solvent (H_2O and D_2O) single-beam spectrum was ratioed against a 4096 scan background single-beam spectrum of air to obtain an absorbance spectrum. Scaled subtraction of the sample and solvent absorbance spectra were done to remove solvent bands using software provided by Mattson Instruments, Inc. An LN_2 -cooled, photovoltaic mercury cadmium telluride detector (Infrared Associates, Inc.) was used, and an intermediate aperture was adjusted to keep the interferogram intensity in a range resulting in not more than 1% detector nonlinearity (a peak-to-peak voltage of not more than 5 V for the detector used). The sample temperature was maintained at $15\text{ }^\circ\text{C}$ using a water-jacketed sample holder connected to a Neslab Endocal RTE-9 refrigerated circulating

bath. Barium fluoride windows were used with inert spacer material providing a nominal path length of $8\text{ }\mu\text{m}$.

Raman spectra were obtained for room temperature aqueous samples in 5 mm quartz test tubes held in a standard NMR tube spinner fitted with a customized Teflon sleeve. Excitation at 647 nm was provided by a Coherent 599 standing wave dye laser using DCM dye. The dye laser was pumped by a Coherent INNOVA 307 continuous-wave argon ion laser configured for multiline operation. Output from the dye laser was passed through a Pellin-Broca prism stage to remove extraneous light prior to illumination of the sample. Backscattered photons from the sample were collected at approximately 60° relative to the excitation beam with an illumination stage providing 2-fold magnification at the entrance slit of a Chromex 500IS single-stage spectrograph equipped with a 1200 groove/mm holographic grating. Rayleigh-scattered photons were rejected mechanically at the spectrograph slit by adjusting the slit height and optically by using a holographic notch filter (Kaiser Optical Systems, Inc.) that was angle-tuned for maximum spectral coverage. The detector was a Princeton Instruments, Inc. LN/CCD-1024TKB LN_2 -cooled, back-thinned, 1024-by-1024 pixel array charge-coupled device (CCD). The detector controller was interfaced to a Gateway2000 486/33C computer with hardware provided by the manufacturer. The CCD Spectrometric Multi-channel Analysis (CSMA) software version 2.2a provided by Princeton Instruments, Inc. was used for all detector control functions. Spectra were calibrated using software based on the ASYST scientific software development package (Asyst Software Technologies) and further developed in the laboratory of Dr. Terry Gustafson (Department of Chemistry, The Ohio State University). A solution of neat ethyl acetate and a 1:1 mixture of benzene and CCl_4 provided a sufficient number of calibration points over the range of $250\text{--}1800\text{ cm}^{-1}$. A quadratic fit to these points served as the calibration function for converting from pixel number on the CCD to wavenumber shift. Raman band center frequencies were determined using the PeakFit program (SPSS, Inc.) running on a PC/DOS platform.

Calculation. The vibrational frequencies and transition intensities were obtained in double harmonic approximation using *ab initio* HF and hybrid HF/DFT-B3LYP formalisms (referred to as DFT-B3LYP throughout).^{23–28} The HF calculations were performed using the 6-31+G* basis set²⁹ while the DFT-B3LYP calculations were performed using the 4-31G basis set.³⁰ From our previous study of uracil,⁷ it was found that calculations done within the DFT-B3LYP formalism at the 6-31+G* level took over four times longer to converge than those done at the 4-31G level. It was also demonstrated that the DFT-B3LYP calculations done at the 4-31G level were more accurate than the HF calculations done at a much higher precision (6-31+G*). With CPU time at a premium, it was deemed that a reasonable tradeoff between execution time and accuracy was to perform DFT-B3LYP calculations with the 4-31G basis set.

The solute–solvent interaction was approximated using both the Kirkwood–Onsager reaction field formalism^{14,15} (as first implemented by Beens and Weller¹⁶ and later expanded by Wong et al.¹⁷) and the SCIPCM (a modified version of the PCM model of Tomasi developed by Wiberg et al.^{18–20}). In the SCM, the radius of the solute spherical cavity was determined from the molecular volume within the electron density contour of $0.001\text{ q}_e/\text{bohr}^3$. For the SCIPCM method, the isosurface level was specified in the range of $0.001\text{--}0.0004\text{ q}_e/\text{bohr}^3$. All reaction field calculations were done with a dielectric constant approximating bulk water at room temperature ($\epsilon = 78.54$). The

TABLE 1: Summary of All Calculations Performed^a

	Raman/H ₂ O	Raman/D ₂ O	Infrared/H ₂ O	Infrared/D ₂ O
HF/DFT 4-31G spher. cavity				
HF/DFT 4-31G SCIPCM				
HF/6-31G* HF/6-31+G* spher. cavity				
HF/6-31G* HF/6-31+G* SCIPCM				

^a The shaded blocks represent complete calculations of all properties shown while unshaded areas represent situations in which one or more calculated properties could not be obtained.

SCM calculations were performed for both N-protonated and N-deuterated species, but implementation problems with Gaussian 94/98 prevented calculations of the N-deuterated species using the SCIPCM method. Calculations were performed using the Gaussian-94/98³² sets of programs running on either the CRI Cray Y-MP8/864 or the T90/4128 supercomputer both controlled by the UNICOS operating system. Further analysis of the Gaussian results was completed on a Digital Equipment Corporation VAXStation 3200 or an Aspen Systems, Inc. Durango 500 alpha system both running the VMS operating system (P. Ilich, unpublished FORTRAN software).

Results and Discussion

Vibrational normal mode assignments have been made for all in-plane vibrational modes of lumazine in the neutral, monoanionic, and dianionic forms in both H₂O and D₂O in the 300–1750 cm⁻¹ region based on the results obtained from both HF/6-31+G* and DFT-B3LYP/4-31G calculations incorporating the Kirkwood–Onsager spherical cavity and the SCIPCM reaction field models. The various steps taken to arrive at these assignments are presented below. In section A, the prototropic equilibria of lumazine in aqueous media are evaluated using two reaction field models. The SCIPCM calculations predict that the A1/N3H form of the monoanion is more stable by approximately 2 kcal than the A3/N1H form in an aqueous medium. However, the SCM calculations predict that the most probable monoanionic species in a high dielectric environment is the A3/N1H form by 9.5 kcal over the A1/N3H form. A comparison of the predicted vibrational frequencies for each of these species with experimental spectra (both Raman and FTIR) indicated that it is the A1/N3H form of the lumazine monoanion that is most prevalent in aqueous solution at neutral pH. Technical difficulties with the Gaussian software using the SCIPCM method preclude calculation of the vibrational frequencies of the N-deuterated tautomers of lumazine; however, results from this model are important in determining correct tautomeric forms for a specific ionization state of lumazine. To assess the utility of isotopic H/D shifts as an aid in making vibrational assignments, the Kirkwood–Onsager SCM model has been used for calculations done on the N-protonated and N-deuterated forms of lumazine determined to predominate at a given pH/pD. In section B, we then compare the predicted vibrational mode frequencies derived from the SCM/DFT-B3LYP/4-31G calculations with experiment. Calculated and observed vibrational mode frequencies are compared for the N1H(D), N3H(D)-neutral, the A1/N3H(D)-monoanion and the A1,A3-dianion forms of lumazine (Tables 2 and 3, sections B.1.1 and B.1.2). This comparison demonstrates that these calculations are reasonably accurate in determining vibrational mode frequencies for each lumazine species studied. It also

proves possible to make correlations between vibrational modes with changes in ionization state. These correlations are obtained by reading across each row of Table 2 (Table 3 for the deuterated species). The strength of the correlations of the individual mode progressions with changes in ionization state is best illustrated in the correlation table in mode plot form (Table 4 for the protonated species and Table 6 for the deuterated species, sections B.2.1 and B.2.2). A quantitative comparison between the predicted and the observed shifts with changes in ionization is shown in Table 5 for the protonated species and Table 7 for the deuterated species. These same shifts are illustrated by comparing the experimental Raman and FTIR data for each species with spectra simulated from the results of the calculations (Figure 1 for protonated lumazine and Figure 2 for deuterated lumazine). Finally, in section C, the H/D isotopic shifts are analyzed for both the neutral and the monoanionic forms of lumazine. Calculated and observed shifts are compared for the neutral and monoanionic species in Tables 8 and 9, respectively. Simulated spectra are compared to experimental Raman spectra for these same species in Figures 3 and 4. Final geometries resulting from full molecular geometry optimizations calculated at the SCM/DFT-B3LYP/4-31G level for neutral, the A1/N3H-monoanion, and the A1,A3-dianion forms of lumazine can be found in Tables 1S, 2S, and 3S, respectively, in Supporting Information in both Cartesian coordinates and Z matrix forms.

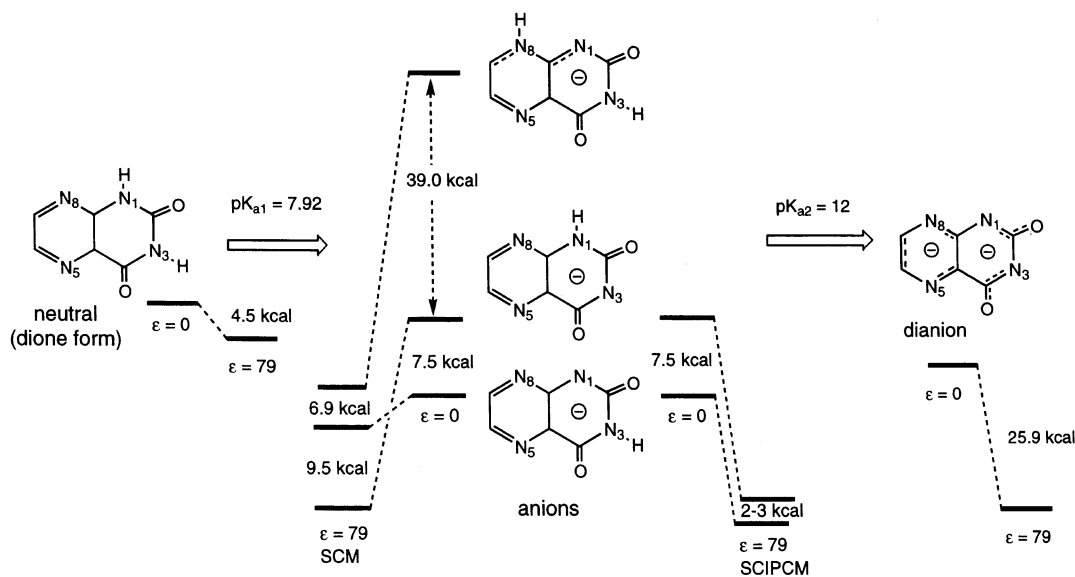
A. Relative Stabilities of Protonation States. Lumazine, 1,4-dioxo-pyrimidino[5,6-c]pyrazine (or, 2,4-(1H,3H)pteridinedione), as cation (protonated), neutral, and monoanion (deprotonated) species, can exist in a variety of prototautomeric forms, and a comprehensive analysis of lumazine as substrate for enzymatically catalyzed oxidative hydroxylation must allow for possible exchange among different forms in the course of reaction. Given the presence of amido, amino, and imino groups in the molecule, lumazine and its monoanions could exist in two canonical forms, as (i) ketaminoketamino or as (ii) enolateenolate prototautomers. Preliminary electronic structure calculations of neutral lumazine, carried out in vacuo with semiempirical AM1,³² MNDO,³³ and PM3³⁴ methods, and Gaussian ab initio HF and DFT methods performed at several levels of theory all indicate that the ketaminoketamino tautomer is the dominant form of neutral and monoanion lumazine species, with the dianion existing in a single form. Subsequent calculations in a simulated aqueous environment (vide infra) support the ketaminoketamino form as the most stable.

The relative stabilities of the various tautomeric forms of lumazine are summarized in Scheme 1. There are three possible lumazine monoanions of the ketamino form; the N8H-monoanion (with the pyrazine moiety containing both the pyrrole and the pyridine type nitrogens) is significantly higher in energy

TABLE 2: Comparison of the Predicted and Observed Vibrational Frequencies for the Neutral, Monoanionic, and Dianionic Forms of N-Protonated Lumazine^{a-e}

neutral (SF = 0.987)				monoanion (unscaled)				dianion (unscaled)			
mode	calcd	obsv	O - C	mode	calcd	obsv	O - C	mode	calcd	obsv	O - C
Q5	1725	1719	6	Q5	1648	1645	3	Q7	1428	1451 (IR)	23
Q6	1709	1703	6	Q4	1699	1683	16	Q3	1593	1579	14
Q7	1574	1589	15								
Q8	1561	1569	8	Q6	1565	1570	5	Q4	1554	NO	
Q9	1510	1516	6	Q7	1534	1535	1	Q5	1528	1533	5
				Q8	1499	1503	4	Q6	1487	1495	8
Q10	1446	1458 (IR)	12	Q9	1424	1422 (IR)	2	Q8	1411	1428 (IR)	17
Q11	1426	1424 (IR)	2								
Q12	1410	1402 (IR)	8								
Q13	1379	1380 (IR)	1	Q10	1399	1406	7	Q9	1374	1392 (IR)	18
Q14	1296	1308	12	Q11	1360	1378	18				
				Q12	1334	1324	10	Q10	1313	1325	12
Q15	1287	1287	0	Q13	1263	1283	20	Q12	1219	1235	16
Q16	1241	1232	9	Q14	1253	1233	20	Q11	1260	1297	37
Q17	1192	1188	4	Q15	1171	1177	6	Q13	1193	1194	1
Q18	1139	1177 (IR)	38	Q16	1124	1142 (IR)	18	Q14	1109	1136 (IR)	27
Q19	1079	1067	12	Q17	1091	1078	13	Q15	1091	1085	6
Q21	1005	NO		Q19	1005	1018	13	Q17	993	1026	33
Q22	927	934	7	Q20	931	937	6	Q18	939	944	5
Q26	797	NO		Q24	796	797	1	Q22	778	NO	
Q30	676	686	10	Q28	664	676	13	Q25	665	687	22
Q31	655	668	13	Q27	688	691	3	Q24	717	NO	
Q33	562	573	11	Q30	563	575	12	Q27	579	593	14
Q34	493	495	2	Q31	515	513	2	Q28	510	525	15
Q36	456	465	9	Q33	464	473	9	Q30	467	483	16
Q37	363	NO		Q34	374	NO		Q31	396	NO	
Q38	300	NO		Q35	313	NO		Q32	315	NO	
avg O - C			9.10	avg O - C			9.18	avg O - C			16.06

^a The scale factor, denoted by SF, is shown in parentheses next to the main section header. ^b All frequencies are in cm⁻¹. ^c Shifts with (de)protonation are correlated by reading across the table rows. ^d |O - C| denotes the absolute value of (observed frequency - calculated frequency), and the average of these unsigned differences is shown at the bottom of each section. ^e NO denotes not observed.

SCHEME 1: Lumazine Two Step Deprotonation^{a,b}

^a All energy differences are from the SCM/HF/6-31+G* calculations except in the case of the anions marked SCIPM (SCIPM/DFT-B3LYP/4-31G). ^b The pK_{a1} value is taken from a pH titration, and the pK_{a2} value is from ref 43.

than the other two isomers in vacuo (39 kcal/mol at the UHF/6-31+G* level), as well as in simulated aqueous environment. The A1/N3H anion isomer is predicted to be sufficiently more stable, by 7–10 kcal/mol, and to be the predominant form of the lumazine anion. In simulated aqueous environment, the energy differences between the N8H, A1/N3H, and A3/N1H isomers decrease to one-half to one-third of that predicted in vacuo, with the separation between the two most stable forms, A1/N3H and A3/N1H, predicted to narrow to 1.6–2.7 kcal/mol, or even become inverted. A similar situation, encountered

in our previous study of uracil,⁷ has been recognized for oxypyrimidine monoanions by other authors.³⁵ The question of the most stable form of the pyrimidinedione anion isomer lies at the heart of the structure, chemistry and biology of the dioxo pyrimidine (uracil/uridine), dioxo and trioxo purine (uric acid and precursors), dioxo and trioxo pteridine (pterin enzyme cofactors), and isalloxazine compounds (flavins), and is therefore an important point. It is possible, however, that there is not a single most stable lumazine anion or not always the same isomer in every medium. For example, a previous study

TABLE 3: Comparison of the Predicted and Observed Vibrational Frequencies for the Neutral, Monoanionic, and Dianionic Forms of N-Deuterated Lumazine^{a-e}

neutral (SF = 0.987)				monoanion (SF = 0.999)				dianion (unscaled)			
mode	calcd	obsv	O - C	mode	calcd	obsv	O - C	mode	calcd	obsv	O - C
Q5	1725	1715	10	Q4	1690	1667	23	Q7	1593	1583	10
Q6	1689	1677	12	Q4	1624	1622	2	Q3	1428	1453 (IR)	25
Q7	1568	1587	19	Q6	1561	1570	9	Q4	1554	NO	
Q8	1559	1556	3	Q7	1532	1534	2	Q5	1528	1530	2
Q9	1503	1506 (IR)	3	Q8	1498	1504	6	Q6	1487	1496	9
Q10	1445	1450	5	Q9	1422	1418	4	Q8	1411	1420	9
Q11	1404	1404	0	Q11	1340	1324	16	Q10	1313	1325	12
Q12	1348	1343	5	Q12	1267	1292	25	Q11	1260	1299	39
Q13	1293	1311	18	Q13	1256	1253	3	Q12	1219	1234	15
Q14	1256	NO		Q14	1205	1234	29	Q13	1193	1192	1
Q15	1236	1255	19	Q15	1142	1149	7	Q14	1109	1132	23
Q16	1188	1183	5	Q16	1119	1120	1	Q18	939	943	4
Q17	1155	1156	1	Q19	964	968	4	Q15	1091	1083	8
Q18	1073	NO		Q17	1067	1048	19	Q17	993	1024	31
Q19	1064	1044	20								
Q22	900	906	6	Q22	874	871	3	Q22	778	NO	
Q24	882	NO		Q24	784	785	1	Q25	665	691	26
Q27	762	NO		Q26	673	691	18	Q24	717	NO	
Q28	677	684	7	Q27	642	663	21	Q27	579	597	18
Q29	620	638	18	Q29	560	574	14	Q28	510	529	19
Q31	559	571	12	Q31	509	510	1	Q30	467	487	20
Q34	484	488	4	Q32	462	474	12	Q31	396	NO	
Q36	455	466	11	Q34	373	NO		Q32	315	NO	
Q37	363	NO		Q35	313	NO					
Q38	300	NO									
avg O - C			9.15	avg O - C			10.77	avg O - C			16.00

^a The scale factor, denoted by SF, is shown in parentheses next to the main section header. ^b All frequencies are in cm⁻¹. ^c Shifts with (de) deuteration are correlated by reading across the table rows. ^d |O - C| denotes the absolute value of (observed frequency - calculated frequency), and the average of these unsigned differences is shown at the bottom of each section. ^e NO denotes not observed.

has demonstrated that the anion isomer of lumazine in aqueous solvent is different from that in dimethyl sulfoxide (DMSO).³⁶ Again, because it is a substrate for enzymatic oxidation and therefore exposed to environments of highly inhomogeneous protonating power, this aspect of lumazine chemistry deserves careful analysis. The problem, unfortunately, becomes complicated somewhat by methodological and procedural limitations of the electronic structure calculations.

The typical regimen of electronic structure calculations starts with low level (sometimes semiempirical) calculations in vacuo, which, after a triage of least likely structures, are repeated at consecutively higher levels of theory (with inclusion of electron correlation correction employing the Becke^{26,27} and Lee, Yang, and Parr formalism²⁸ within the DFT method). After full geometry optimization, the Hessian matrix is then calculated yielding harmonic vibrational energies, vibrational force constants, and infrared (first order) and Raman (second order) vibrational transition strengths. The last two steps, involving structure optimization and the Hessian matrix calculation, are then repeated for a simulated environment. This procedure has been applied to each lumazine species presented here (see Scheme 1). In our study of uracil,⁷ we employed the Kirkwood-Onsager spherical cavity method^{14,15} and the isodensity potential surface model.¹⁸⁻²⁰ With both methods, the environment is a perfectly homogeneous "jellium" and only the scalar dielectric constant sets its character toward more polar (e.g., $\epsilon_0 = 78.5$, as in water) or less polar (e.g., $\epsilon_0 = 1.54$, as in an argon matrix); the difference between the two methods is in the shape of the cavity. The isodensity envelope, created according to the molecular shape and charge distribution (and set to a predetermined level, typically 1/100 of electron charge), is expected a priori to be a more realistic model but is far more computationally intensive than the Kirkwood-Onsager model. However,

little difference has been observed between the two methods in the case of uracil, possibly due to the fairly symmetric, approximately circular overall shape of the molecule. On the basis of the same argument, more significant differences might be expected in the case of a less spherical molecule like lumazine, and indeed, this is what has been observed in the ordering of anion isomers by thermodynamic stability. Using the spherical cavity Kirkwood-Onsager solvation model with various cavity diameters ("tight" shell, "nominal" and "loose" shell; see the details in ref 7), the most stable isomers become inverted on going from vacuum to a continuum with a dielectric constant of 78.5, at several levels of HF and DFT full energy optimizations (4-31G, 6-31G*, and 6-31+G*), with the A1/N3H isomer predicted to be 7-8 kcal/mol lower in energy (B3LYP/4-31G, UHF/6-31+G*) than the A3/N1H form (the most stable isomer in vacuo is expected to become less stable than the A3/N1H isomer in a high-dielectric constant spherical cavity by 9-10 kcal/mol). Normal mode analysis of our experimental and calculated Raman spectra of lumazine species at various pH/pD values, however, supports the energy ordering predicted by calculations employing the SCIPCM solvation model, according to which the A3/N1H and A1/N3H anions become closer in energy in the high dielectric constant continuum but do not reverse in order as shown in Scheme 1. The energy ordering of lumazine anions in a simulated aqueous environment, with A1/N3H being 2-3 kcal/mol more stable than the A3/N1H isomer, is closely corroborated by our subsequent calculations using the ab initio GAMESS set of programs³⁷ including the SM5.42R solvation model in GAME-SOL V3.0³⁸ (data not shown). We conclude that the A1/N3H isomer is the dominant lumazine anion form at pH/pD above the first pK_a for lumazine as determined by spectrophotometric titration (pK_{a1} ~ 7.92, in close agreement with previously

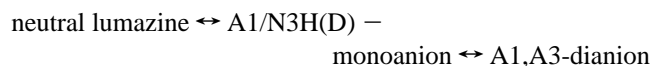
TABLE 4: Mode Plots of the Correlations of Vibrational Modes for the N-Protonated Forms of Lumazine Predicted by the SCM/DFT-B3LYP/4-31G Calculations

Lumazine Neutral	Lumazine Monoanion	Lumazine Dianion	Lumazine Neutral	Lumazine Monoanion	Lumazine Dianion

TABLE 4: (Continued)

Lumazine Neutral	Lumazine Monoanion	Lumazine Dianion	Lumazine Neutral	Lumazine Monoanion	Lumazine Dianion

reported values³⁹). On the basis of this analysis, for the pH/pD range considered in this study, the lumazine two step deprotonation proceeds by the following scheme:



B. Vibrational Frequency Calculations vs Experiment. As described in section A, the protonation states expected over the pH/pD range studied are the N1H(D), N3H(D)-neutral, the A1/N3H(D)-monoanion, and the A1,A3-dianion forms of lumazine. To have as much experimental vibrational information as possible, we have collected both scattering Raman spectra and infrared spectra in aqueous media at several pH/pD values (pH 2.2, 11.0, 13.0 and pD 4.9, 8.9, 13.0). For comparison, we have also calculated the vibrational frequencies and both the infrared transition strengths and the Raman scattering intensities for each of these forms. All SCRF vibrational frequency and infrared intensity calculations have been carried out using the SCM/DFT-B3LYP/4-31G method. Raman scattering intensities have been determined from a separate set of calculations done with the SCM/HF/6-31+G* method since second order transition moments are not available in a DFT/SCM calculation using the Gaussian program suite.

At a relatively low level of theory, the Pople 4-31G basis set,³⁰ with inclusion of the DFT treatment of electron correlation,^{23–25} has been shown to perform quite well in the

calculation of energies and reasonably well in the calculation of transition moments for the in-plane vibrational modes for cation, neutral, anion, and dianion forms of pyrimidinedione (uracil);⁷ the same method has been found here to be reliable and economical for the calculation of the vibrational energies and transition strengths for all lumazine species in vacuo and in a simulated aqueous environment. Because of current limitations in theory,³¹ no second order transition moments could be calculated within the DFT/SCM (nor within the MP perturbation) method. While basing our analysis of energies and harmonic modes on the results obtained by DFT calculations, we have analyzed the Raman intensities with the help of second order transition moments obtained from HF calculations (at the HF/6-31G* and HF/6-31+G* levels) carried out for some lumazine species. In addition, the current procedural/coding deficiencies in the GAUSSIAN set of programs necessitated further concessions in the use of solvation models for isotopically labeled lumazine species. As no isotopic replacement calculations could be carried out within the SCIPCM model (probably due to faulty checkpoint alignment when reading the Cartesian force field matrix and vibrational frequencies), the analysis of the isotopic shifts while based on the DFT/SCIPCM calculations also employed the frequency shifts calculated within the Kirkwood–Onsager solvation model with the spherical cavity radius set at $0.85a_0$ (referred to as the tight shell in ref 7). In Table 1, the shaded areas represent complete calculations

TABLE 5: Comparison of the Calculated and Observed Neutral-to-Monoanion (N-to-M) and Monoanion-to-Dianion (M-to-D) Shifts for the N-Protonated Lumazine Mode Progressions^a

mode progression			calcd shifts (cm ⁻¹)		obsv shifts (cm ⁻¹)	
neutral	monoanion	dianion	N-to-M	M-to-D	N-to-M	M-to-D
Q5	Q5	Q7	-77	-220	-74	-194
Q6	Q4	Q3	-10	-106	-20	-104
Q8	Q6	Q4	+4	-11	+1	NO
Q9	Q7	Q5	+24	-6	+19	-2
	Q8	Q6		-12		-8
Q10	Q9	Q8	-22	-13	-36	+6
Q13	Q10	Q9	+20	-25	+25	-13
Q14	Q11		+64		+70	
	Q12	Q10		-21		+1
Q15	Q13	Q12	-24	-44	-4	-48
Q16	Q14	Q11	+12	+7	+1	+64
Q17	Q15	Q13	-21	+22	-11	+17
Q18	Q16	Q14	-15	-15	-35	+7
Q19	Q17	Q15	+12	0	+11	+7
Q21	Q19	Q17	0	-12	NO	+8
Q22	Q20	Q18	+4	+8	+3	+7
Q26	Q24	Q22	-1	-18	NO	NO
Q30	Q28	Q25	-12	+1	-10	+11
Q31	Q27	Q24	+33	+29	+23	NO
Q33	Q30	Q27	+1	+16	+2	+18
Q34	Q31	Q28	+22	-5	+18	+12
Q36	Q33	Q30	+8	+3	+8	+10
Q37	Q34	Q31	+11	+22	NO	NO
Q38	Q35	Q32	+13	+2	NO	NO

^a NO denotes not observed.

of all properties (the basis set, the method, the solvation model, and the isotopic replacement) while each unshaded area depicts a situation in which one or more calculated properties (e.g., Raman intensities, SCIPCM solvation model, H/D effects) could not be obtained with a given basis set or the method (HF or DFT), and as explained in the text, some of the properties had to be "borrowed" from similar calculations performed with a different basis set (4-31G vs 6-31+G*) or a different method (HF vs DFT). The technical and procedural complications notwithstanding, we were able to combine the energy, second order transition moments, and isotopic shifts in solvated lumazines, calculated at several levels of theory, into a fairly congruent picture of the harmonic molecular vibrations of lumazine species in aqueous media at different pH/pD values.

Lumazine belongs to the C_s point group. The neutral species contains 42 fundamental modes of vibration (29 a' in-plane modes and 13 a'' out-of-plane modes), the monoanion contains 39 fundamental modes (27 a' in-plane modes and 12 a'' out-of-plane modes), and the dianion contains 36 fundamental modes (25 a' in-plane modes and 11 a'' out-of-plane modes). In the energy regions that we have examined (300–1750 cm⁻¹ with Raman and 1000–1750 cm⁻¹ with FTIR), it is expected that the in-plane modes will predominate. From the reaction field calculations, only a single out-of-plane mode is predicted in the 1000–1750 cm⁻¹ range and its calculated IR intensity is very weak (and indeed there is no corresponding band discernible in the FTIR data, see below). In general, the out-of-plane mode Raman intensities are also predicted to be quite weak. For these reasons, the normal mode analysis that follows is limited to the in-plane modes of each lumazine species considered.

B.1. Accuracy of Calculations. As a measure of the performance of the theoretical method used for vibrational mode assignments in this study (the SCM/DFT-B3LYP/4-31G method), a direct comparison of the experimentally observed vibrational frequencies with those obtained theoretically is given in Tables 2 and 3 for the N1-H(D)/N3-H(D) neutral, A1/N3-H(D)

monoanion and dianion forms of lumazine. Included in these tables are the unsigned differences between experimental and scaled theoretical vibrational frequencies as well as the average unsigned error for each species. The scale factor for each set of data has been chosen as the factor that resulted in the lowest average unsigned error for vibrational modes in the 300–1750 cm⁻¹ range. In two of the five cases, the calculated frequencies were used unscaled and the other three scale factors were very close to one (0.987 for protonated neutral, 0.990 for deuterated neutral, and 0.999 for deuterated monoanion). A variety of scaling methods have been employed by other workers including the SQM force field method with internal coordinate transformations of Pulay⁴⁰ and the scaling procedure of Martin et al. in which three separate scale factors were used in the study of a group of polycyclic aromatic compounds (naphthalene, azulene, phenanthrene, and anthracene), with the C–H stretches scaled by 0.960, the in-plane bends by 0.983, and all remaining vibrations by 0.970 when employing the DFT/cc-pVDZ level of theory. In the same study, only two scale factors were found necessary when the calculations were done at the DFT/cc-VTZ level of theory: the C–H stretches were scaled by 0.965 and all other vibrations by 0.975.⁴¹ These scaling methods resulted in reproduction of the fundamental frequencies of the molecules studied to within 10 cm⁻¹ or better. Another study on the molecular vibrations of pteridine, 1,4,5,8-tetraazaphthalene, and 2,3,6,7-tetraazaphthalene compared results from calculations done at various levels of theory (HF/6-31G*, MP2/6-31G*, B3LYP/4-31G, and B3LYP/6-31G*) with experiment.⁴² Single scale factors were applied to the calculated vibrational frequencies from each level of theory with the best overall fit to the data coming from the B3LYP calculations. The mean deviation of the difference between experimental and calculated frequencies for these derivatives ranged from 7 to 12 cm⁻¹ at the B3LYP/6-31G* level and from -4 to 18 cm⁻¹ at the B3LYP/4-31G level. The B3LYP/4-31G calculations were found to be satisfactory in terms of goodness of fit and required less than half the CPU time of the 6-31G* set, although the accuracy of the calculations may have resulted from a cancellation of errors.

Using a simple scale factor applied to the calculated in-plane vibrational frequencies for each lumazine species considered in this study results in an average unsigned error range of 9.10–16.06 cm⁻¹. This degree of accuracy is satisfactory for further vibrational frequency analysis and mode assignments.

B.1.1. Protonated Forms of Lumazine. A direct comparison of the observed and calculated vibrational frequencies for the N-protonated forms of lumazine in the 300–1750 cm⁻¹ region is given in Table 2. Of the 25 in-plane modes expected from calculations for the neutral species in this energy region, only 21 modes can be assigned in the experimental spectra. The unsigned differences between the observed and the calculated frequencies range from 0 cm⁻¹ for Q15 to 38 cm⁻¹ for Q18 with the average unsigned difference for the set being 9.10 cm⁻¹. For the A1/N3-H monoanion, 22 of the 24 theoretical in-plane modes can be assigned in the experimental spectra, with the unsigned differences in this set ranging from 1 (Q7, Q24) to 20 cm⁻¹ (Q13, Q14) with an average unsigned difference of 9.18 cm⁻¹. In the case of the dianion, 18 of the 23 in-plane modes can be assigned in the experimental high pH spectra. The unsigned differences range from 1 (Q13) to 37 cm⁻¹ (Q11) with an average unsigned difference of 16.06 cm⁻¹.

B.1.2. Deuterated Forms of Lumazine. A comparison between observed and calculated frequencies for the N-deuterated forms of lumazine in the 300–1750 cm⁻¹ region is given in Table 3. Of the 25 in-plane modes expected from

TABLE 6: Mode Plots of the Correlations of Vibrational Modes for the N-Deuterated Forms of Lumazine Predicted by the SCM/DFT-B3LYP/4-31G Calculations

Lumazine Neutral	Lumazine Monoanion	Lumazine Dianion	Lumazine Neutral	Lumazine Monoanion	Lumazine Dianion

TABLE 6: (Continued)

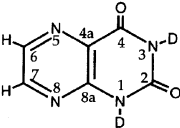
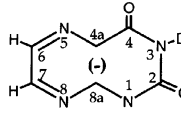
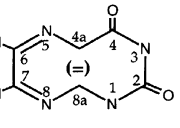
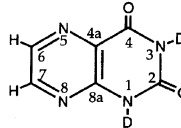
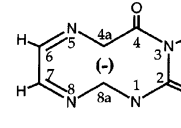
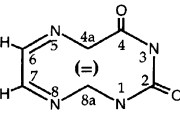
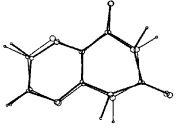
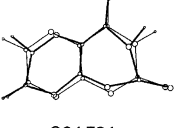
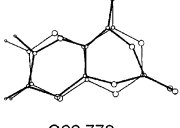
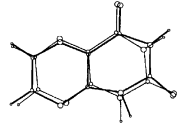
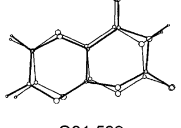
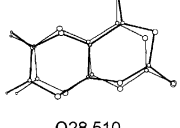
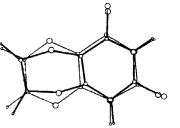
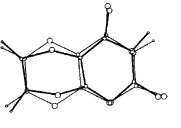
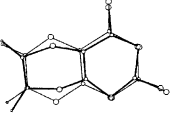
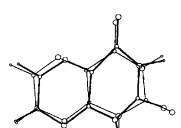
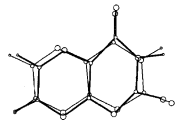
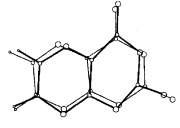
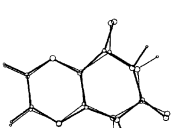
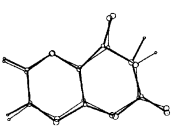
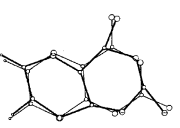
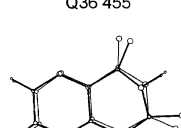
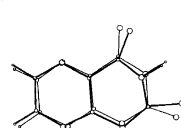
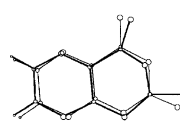
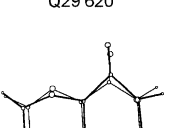
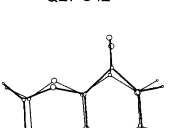
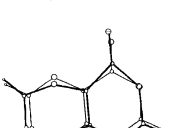
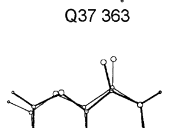
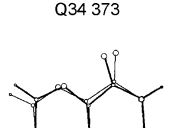
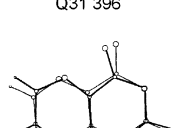
Lumazine Neutral	Lumazine Monoanion	Lumazine Dianion	Lumazine Neutral	Lumazine Monoanion	Lumazine Dianion
					
					
					
					
					

TABLE 7: Comparison of the Calculated and Observed Neutral-to-Monoanion (N-to-M) and Monoanion-to-Dianion (M-to-D) Shifts for the N-Deuterated Lumazine Mode Progressions^a

mode progression			calcd shifts (cm ⁻¹)		obsv shifts (cm ⁻¹)	
neutral	monoanion	dianion	N-to-M	M-to-D	N-to-M	M-to-D
Q5	Q6	Q3	-35	-97	-48	-84
Q6	Q5	Q7	-65	-196	-55	-169
Q7	Q6	Q4	-7	-20	-17	NO
Q8	Q6		+2		+14	
Q9	Q7	Q5	+29	-4	+28	-4
Q9	Q8	Q6	-5	-11	-2	-8
Q10	Q9	Q8	-23	-11	-32	+2
Q11	Q9		+18		+14	
	Q10	Q9		-13		-13
Q12	Q11	Q10	-8	-27	-19	+1
Q13	Q11		+47		+13	
Q14	Q12	Q11	+11	-7		+7
	Q13	Q12		-37		-19
	Q14	Q13		-12		-42
Q15	Q14		-31		-21	
Q16	Q15		-46		-34	
Q17	Q16	Q14	-36	-10	-36	+12
Q18	Q19	Q18	-109	-25	NO	-25
Q19	Q17	Q15	+3	+24	+4	+35
Q24	Q22	Q18	-8	+69	NO	+72
Q27	Q24	Q22	+22	-6	NO	NO
Q28	Q26	Q25	-4	-8	+7	0
Q29	Q27	Q24	+22	+75	+25	NO
Q31	Q29	Q27	+1	+19	-3	+23
Q34	Q31	Q28	+25	+1	+22	+19
Q36	Q32	Q30	+7	+5	+8	+13
Q37	Q34	Q31	+10	+23	NO	NO
Q38	Q35	Q32	+13	+2	NO	NO

^a NO denotes not observed.

calculations for the neutral species in this energy region, only 19 modes can be assigned in the experimental spectra. The

unsigned differences between the observed and the calculated frequencies range from 0 cm⁻¹ for Q11 to 20 cm⁻¹ for Q19 with the average unsigned difference for the set being 9.37 cm⁻¹. For the A1/N3-D monoanion, 22 of the 24 theoretical in-plane modes can be assigned in the experimental spectra, with the unsigned differences in this set ranging from 1 (Q16, Q31) to 29 cm⁻¹ (Q14) with an average unsigned difference of 10.77 cm⁻¹. In the case of the dianion, 18 of the 23 in-plane modes can be assigned in the experimental high pH spectra. The unsigned differences ranged from 1 (Q13) to 39 cm⁻¹ (Q11) with an average unsigned difference of 16.00 cm⁻¹.

B.2. Mode Correlations with Changes in Ionization. B.2.1. Protonated Forms of Lumazine. Shifts with (de)protonation are summarized in Table 5 for the N-protonated forms of lumazine. The experimental Raman and infrared spectra are compared with simulated spectra in Figure 1A–D. In the 300–1750 cm⁻¹ region, the largest frequency shifts induced by changes in the protonation state of the molecule are expected in the carbonyl stretching region. The highest energy carbonyl mode in the neutral species, Q5 predicted at 1725 cm⁻¹, is an in-phase C2=O/C4=O stretching mode dominated by C2=O, coupled with N1H and N3H bending motions. The mode that most closely correlates with this carbonyl mode in the monoanion is Q5 (dominated by the C2=O stretch coupled to an N3H bend), with a predicted frequency of 1648 cm⁻¹, reflecting a downshift of 77 cm⁻¹. In the dianion, the mode consisting of a large C2=O stretching component is Q7 at a predicted energy of 1428 cm⁻¹, reflecting a downshift of 220 cm⁻¹ relative to Q5 of the monoanion. The observed shifts for these modes agree quite closely with experiment, with downshifts of 74 cm⁻¹ for the neutral to monoanion and 194 cm⁻¹ for the monoanion to

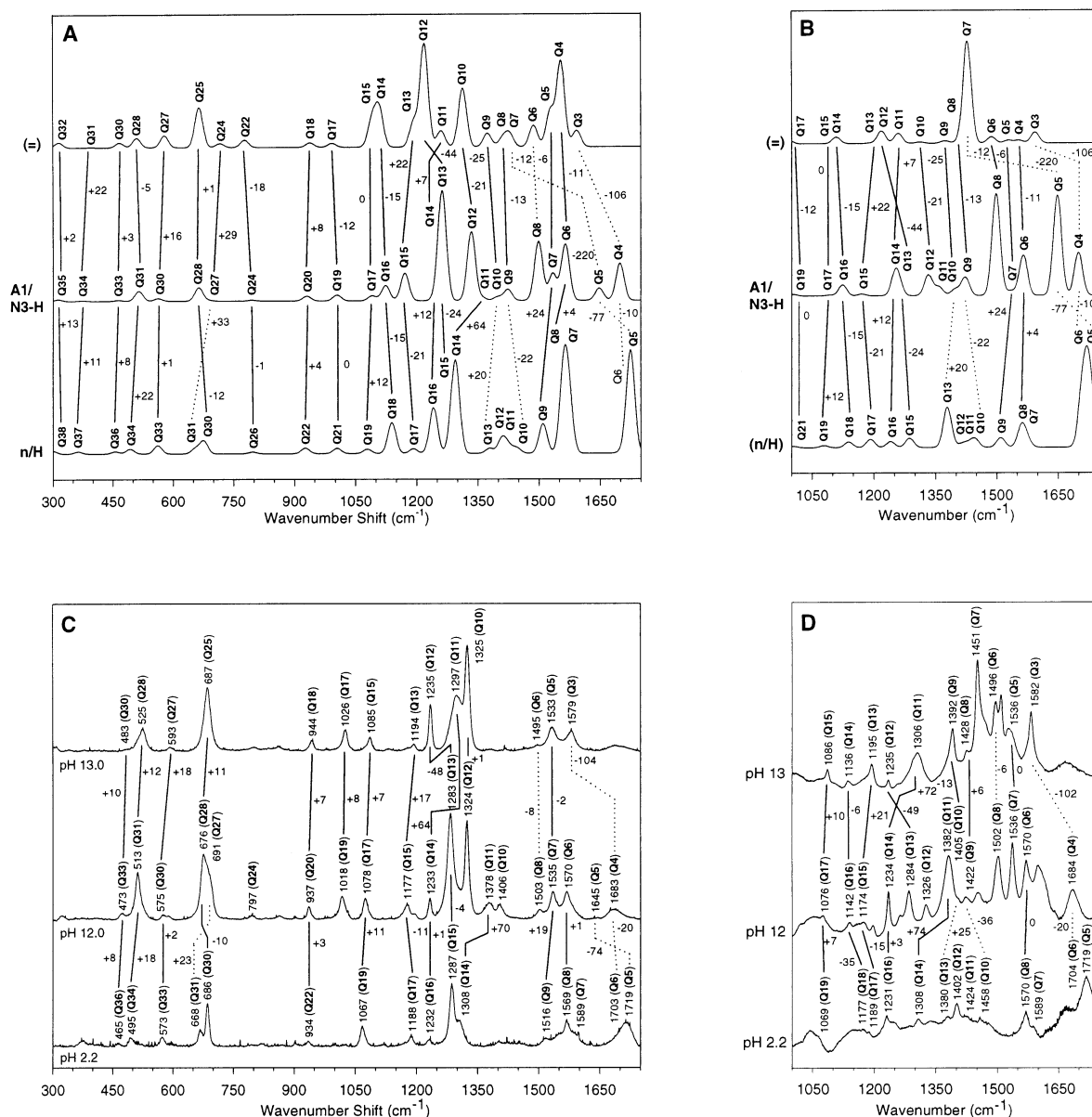


Figure 1. Comparison of (A) simulated Raman and (B) simulated infrared spectra with (C) experimental Raman and (D) experimental FTIR spectra illustrating strong correlations (solid lines) and approximate correlations (dotted lines) for the N-protonated lumazines. Each band is labeled with the appropriate mode number in the simulated spectra and mode number and frequency in the experimental spectra. Each correlation line is also labeled with the corresponding frequency shift. In the simulated spectra, n/H denotes neutral lumazine, A1/N3-H denotes the monoanion, and = denotes the dianion. All simulated spectral bands are enveloped in 20 cm^{-1} fwhm Gaussians. All center frequencies and infrared band intensities are taken from SCM/DFT-B3LYP/4-31G calculations. All Raman band intensities are taken from SCM/HF/6-31+G* calculations.

dianion. For the carbonyl modes dominated by the C4=O stretch, the predicted shifts are from Q6 in the neutral form at 1709 cm^{-1} to Q4 in the monoanion at 1699 cm^{-1} (a downshift of 10 cm^{-1}) to Q3 in the dianion at 1593 cm^{-1} (a downshift of 106 cm^{-1}). The observed shifts for these modes, -20 and -104 cm^{-1} , respectively, again agree quite well with the predicted energy shifts. Detailed mode correlations made in this energy region can be compared by reading across the first two rows of Table 4.

In the 1200–1600 cm^{-1} region, 10 a' fundamental modes (Q7–Q16) are predicted at frequencies of 1574, 1561, 1510, 1446, 1426, 1410, 1379, 1296, 1287, and 1241 cm^{-1} . In the Raman spectrum of the neutral species (Figure 1C, pH 2.2), six prominent bands are observed in this energy region while eight bands are seen in the infrared spectrum (Figure 1D, pH 2.2). Modes Q10–Q13 are not observed in the Raman spectrum while modes Q9 and Q15 are not seen in the infrared spectrum

for the neutral species of lumazine. In this same energy region in the monoanion, nine a' fundamentals are expected, Q6–Q14, at the frequencies 1565, 1534, 1499, 1424, 1399, 1360, 1334, 1263, and 1253 cm^{-1} . In the infrared spectrum of the monoanion (Figure 1D, pH 12), nine bands are observed in this region and all but Q9 are also seen in the Raman spectrum (Figure 1C, pH 12). For the dianion, eight a' fundamentals are expected in this region excluding the carbonyl bands (Q3 and Q7) already discussed. These bands are Q4–Q6 and Q8–Q12 at the frequencies 1554, 1528, 1487, 1411, 1374, 1313, 1260, and 1219 cm^{-1} . Six bands are seen in the infrared spectrum (Figure 1D, pH 13) (Q4 and Q10 are missing), and only five bands are seen in the Raman spectrum (Figure 1C, pH 13) (Q4, Q8, and Q9 are missing). The Q4 mode in the dianion, expected at 1554 cm^{-1} , is the only mode in this energy region not seen experimentally. From Table 4, it can be seen that several modes in the neutral species have no homologues in the monoanion

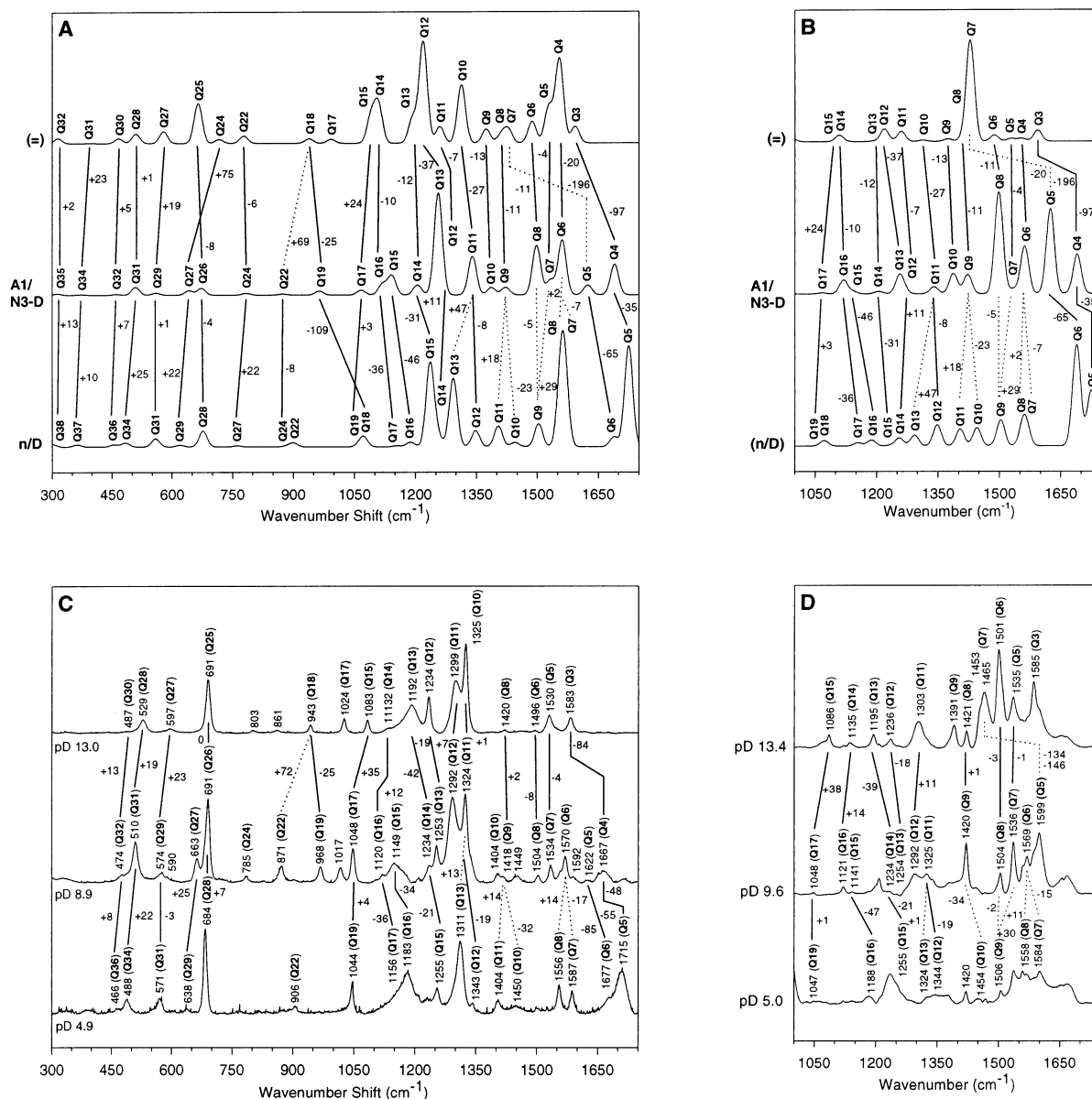


Figure 2. Comparison of (A) simulated Raman and (B) simulated infrared spectra with (C) experimental Raman and (D) experimental FTIR spectra illustrating strong correlations (solid lines) and approximate correlations (dotted lines) for the N-deuterated lumazines. Each band is labeled with the appropriate mode number in the simulated spectra and mode number and frequency in the experimental spectra. Each correlation line is also labeled with the corresponding frequency shift. In the simulated spectra, n/D denotes neutral lumazine, A1/N3-D denotes the monoanion, and = denotes the dianion. All simulated spectral bands are enveloped in 20 cm^{-1} fwhm Gaussians. All center frequencies and infrared band intensities are taken from SCM/DFT-B3LYP/4-31G calculations. All Raman band intensities are taken from SCM/HF/6-31+G* calculations.

or dianion forms (column 1: Q7, Q11, and Q12). Modes Q7 and Q11 have very strong N1H bending components coupled to a CC stretch and C6H/C7H bend in the case of Q7 and a strong C7H bend in the case of Q11. The pyrimidine ring distortion coupled to the N1H bend in mode Q7 is reminiscent of mode Q7 seen in neutral uracil.⁷ Q12 is composed of mostly N3H bend with a small N1H bending component. In this energy region, there is generally close agreement between predicted and observed shifts with ionization. The largest discrepancies are for two monoanion-to-dianion shifts: Q12 to Q10 and Q14 to Q11. Modes Q12 (1324(R)/1326(IR) cm^{-1}) and Q14 (1233-(R)/1234(IR) cm^{-1}) are very prominent in both the Raman and the FTIR spectra for lumazine monoanion prepared at pH 12 (see Figure 1C,D). Predicted shifts for the dianion would put Q10 at approximately 1304 cm^{-1} and Q11 at 1240 cm^{-1} . In the high pH experimental spectra, there are two strong peaks at 1297 and 1325 cm^{-1} in the Raman spectrum and a single, broad

peak centered at 1306 cm^{-1} in the FTIR spectrum. If the higher frequency band in the dianion is assigned to Q10 and the lower to Q11, the experimental shifts are Q12 to Q10, +1 cm^{-1} , and Q14 to Q11, +64 cm^{-1} , predicted to be -21 and +7 cm^{-1} , respectively. If, however, the 1297/1306 cm^{-1} band is assigned as Q10, the Q12 to Q10 shift now falls in the range of -20 to -27 cm^{-1} , very close to the predicted shift. The problem with this assignment is that mode Q11 in the experimental spectra for the dianion remains unassigned.

The 300–1200 cm^{-1} region contains 13 predicted a' fundamental modes for all lumazine species considered in this study. In the neutral species, only nine bands are seen in the experimental data: Q21, Q26, and the two lowest energy modes, Q37 and Q38, are not observed in the Raman and FTIR spectra. These modes are all predicted to have weak Raman scattering intensities from the SCM/HF/6-31+G* calculations. The FTIR spectra of lumazine in aqueous solvent are limited to a low

TABLE 8: Comparison of the Calculated and Observed H/D Isotopic Shifts for the Vibrational Modes of Neutral Lumazine^{a,b}

mode	calcd H	mode	calcd D	D-H	mode	obsv H	mode	obsv D	D-H
Q5	1725	Q5	1725	0	Q5	1719	Q5	1715	-4
Q6	1709	Q6	1689	-20	Q6	1703	Q6	1677	-26
Q7	1574	Q7	1568	-6	Q7	1589	Q7	1587	-2
Q8	1561	Q8	1559	-2	Q8	1569	Q8	1556	-13
Q9	1510	Q9	1503	-7	Q9	1516	Q9	1506 (IR)	-10
Q10	1446	Q10	1445	-1	Q10	1458 (IR)	Q10	1450	-8
Q11	1426				Q11	1424 (IR)			
Q12	1410				Q12	1402 (IR)			
Q13	1379	Q11	1404	+25	Q13	1380 (IR)	Q11	1404	+24
Q14	1296	Q12	1348	+52	Q14	1308	Q12	1343	+35
Q15	1287	Q13	1293	+6	Q15	1287	Q13	1311	+24
Q16	1241	Q14	1256	+15	Q16	1232	Q14		
		Q15	1236	-5			Q15	1255	+23
Q17	1192	Q16	1188	-4	Q17	1188	Q16	1183	-5
Q18	1139	Q17	1155	+16	Q18	1177 (IR)	Q17	1156	-21
		Q18	1073	-66			Q18	NO	
Q19	1079	Q19	1064	-15	Q19	1067	Q19	1044	-23
Q21	1005	Q24	882	-123	Q21	NO	Q24	NO	
Q22	927	Q22	900	-27	Q22	934	Q22	906	-28
Q26	797	Q27	762	-35	Q26	NO	Q27	NO	
Q30	676	Q28	677	+1	Q30	686	Q28	684	-2
Q31	655	Q29	620	-35	Q31	668	Q29	638	-2
Q33	562	Q31	559	-3	Q33	573	Q31	571	-2
Q34	493	Q34	484	-9	Q34	495	Q34	488	+1
Q36	456	Q36	455	-1	Q36	465	Q36	466	+1
Q37	363	Q37	363	0	Q37	NO	Q37	NO	
Q38	300	Q38	300	0	Q38	NO	Q38	NO	

^a All numbers in cm^{-1} . ^b D-H denotes the difference between the N-deuterated frequency and the N-protonated frequency.

TABLE 9: Comparison of the Calculated and Observed H/D Isotopic Shifts for the Vibrational Modes of the Lumazine A1/N3-H(D) Monoanion^{a,b}

mode	calcd H	mode	calcd D	D-H	mode	obsv H	mode	obsv D	D-H
Q4	1699	Q4	1690	-9	Q4	1683	Q4	1667	-16
Q5	1648	Q5	1624	-24	Q5	1645	Q5	1622	-23
Q6	1565	Q6	1561	-4	Q6	1570	Q6	1570	0
Q7	1534	Q7	1532	-2	Q7	1535	Q7	1534	-1
Q8	1499	Q8	1498	-1	Q8	1503	Q8	1504	+1
Q9	1424	Q9	1422	-2	Q9	1422 (IR)	Q9	1418	-4
Q10	1399	Q10	1387	-12	Q10	1406	Q10	1404	-2
Q11	1360				Q11	1378			
Q12	1334	Q11	1340	+6	Q12	1324	Q11	1324	0
		Q12	1267				Q12	1292	
		Q13	1256				Q13	1253	
Q13	1263				Q13	1283			
Q14	1253				Q14	1233			
		Q15	1142	-29			Q15	1149	-28
Q16	1124	Q16	1119	-5	Q16	1142 (IR)	Q16	1120	-22
Q17	1091	Q17	1067	-24	Q17	1078	Q17	1048	-30
Q19	1005				Q19	1018			
		Q19	964				Q19	968	
Q20	931	Q22	874	-57	Q20	937	Q22	871	-66
Q24	796	Q24	784	-12	Q24	797	Q24	785	-12
Q27	688	Q26	673	-15	Q27	691	Q26	691	0
		Q27	642	-46			Q27	663	-28
Q28	664	Q26	673	+9	Q28	676	Q26	691	+15
		Q27	642	-22			Q27	663	-13
Q30	563	Q29	560	-3	Q30	575	Q29	574	-1
Q31	515	Q31	509	-6	Q31	513	Q31	510	-3
Q33	464	Q32	462	-2	Q33	473	Q32	474	+1
Q34	374	Q34	373	-1	Q34	NO	Q34	NO	
Q35	313	Q35	313	0	Q35	NO	Q35	NO	

^a All numbers in cm^{-1} . ^b D-H denotes the difference between the N-deuterated frequency and the N-protonated frequency.

energy cutoff of approximately 1000 cm^{-1} due to strong solvent absorption as well as the natural detector cutoff. For the monoanion, 11 bands are assigned in this region with only the

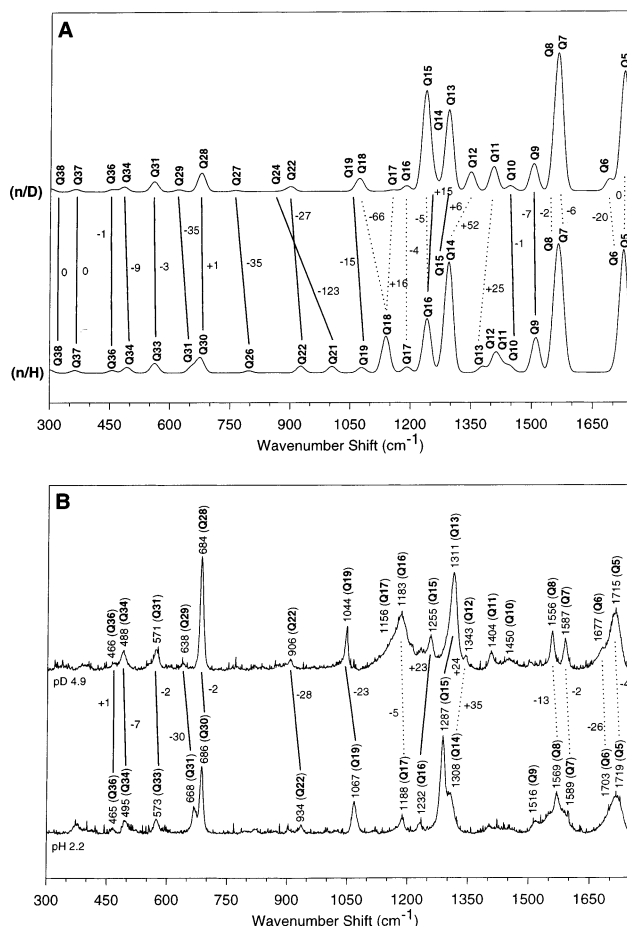


Figure 3. Correlation of the H/D isotopic shifts for (A) simulated Raman spectra and (B) experimental Raman spectra for the neutral forms of lumazine. Strong mode correlations are shown as solid lines and approximate correlations as dotted lines. Each correlation line is labeled with the corresponding H/D shift magnitude. n/H denotes N-protonated lumazine, and n/D denotes N-deuterated lumazine.

two lowest energy modes (Q34 and Q35) not seen in the experimental data. In the dianion, only nine modes can be assigned in the experimental spectra: Q22, Q24, Q31, and Q32 are not seen experimentally. The predicted correlated shifts upon ionization are very close to those observed experimentally in this energy region. The neutral-to-monoanion shifts agree quite closely in both direction of shift and magnitude. For the monoanion-to-dianion shifts, agreement is generally acceptable, but a few correlations do not compare so favorably: the Q19 to Q17 shift is predicted to be -12 cm^{-1} but as assigned in the Raman spectra is $+8 \text{ cm}^{-1}$, and the Q31 to Q28 shift is predicted to be -5 cm^{-1} but is seen in the Raman spectra as $+12 \text{ cm}^{-1}$. For the neutral-to-monoanion correlations, shifts are predicted from -77 to $+64 \text{ cm}^{-1}$ and are observed from -74 to $+70 \text{ cm}^{-1}$ with an average unsigned error of 7 cm^{-1} for the 18 modes observed. The monoanion-to-dianion shifts do not compare as favorably with an average unsigned error of 12.6 cm^{-1} for the 18 modes observed for comparison with calculations. This is still a reasonable error with predicted shifts ranging from -220 to $+29 \text{ cm}^{-1}$ and observed shifts ranging from -194 to $+64 \text{ cm}^{-1}$.

B.2.2. Deuterated Forms of Lumazine. Calculated and observed shifts upon ionization for the N-deuterated forms of lumazine are summarized in Table 7. Simulated Raman and infrared spectra for the neutral, monoanion, and dianion forms of lumazine are compared with experiment in Figure 2A–D. As with the protonated forms, large downshifts are expected

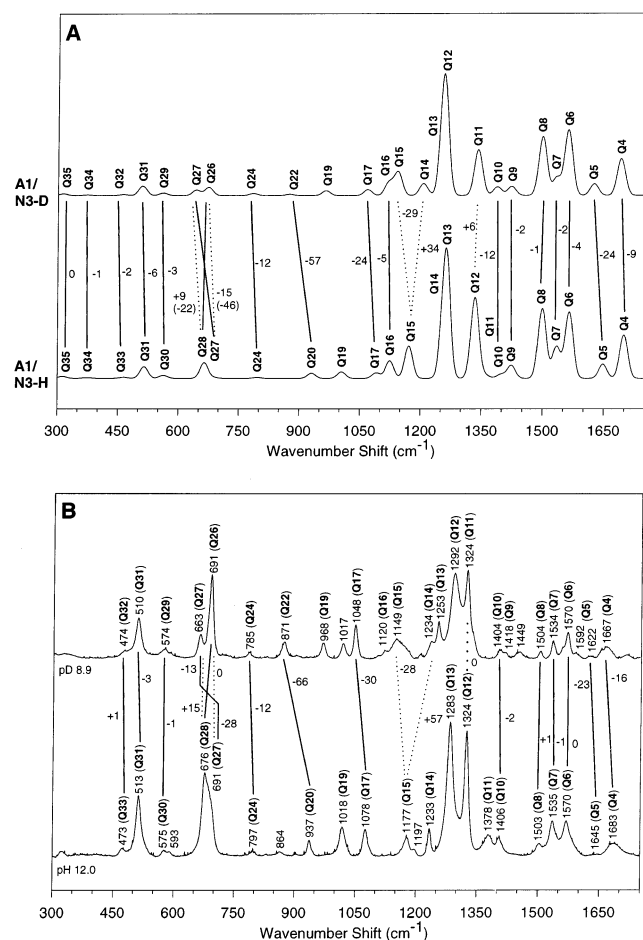


Figure 4. Correlation of the H/D isotopic shifts for (A) simulated Raman spectra and (B) experimental Raman spectra for the A1/N3-H(D) forms of lumazine. Strong mode correlations are shown as solid lines, and approximate correlations are shown as dotted lines. Each correlation line is labeled with the corresponding H/D shift magnitude. A1/N3-H denotes N-protonated lumazine, and A1/N3-D denotes N-deuterated lumazine.

for the carbonyl stretches on going from neutral to monoanion to dianion. The highest energy carbonyl mode in the neutral species is Q5 (analogous to the protonated case) with a predicted frequency of 1725 cm^{-1} . This mode is best described as an in-phase C2=O/C4=O stretch with only a very slight N1H bending component (see Table 6 for details). The corresponding mode in the monoanion that most closely correlates with this mode is Q4 with a calculated frequency of 1690 cm^{-1} , an in-phase C2=O/C4=O stretch but dominated by the C4=O stretching component with only a very slight N3H bending component. This correlation corresponds to a predicted downshift of 35 cm^{-1} . Mode Q3 in the dianion, with a predicted frequency of 1593 cm^{-1} , is also composed of a C2=O/C4=O in-phase stretching component dominated by the C4=O stretch. This corresponds to a further downshift of 97 cm^{-1} relative to Q4 of the monoanion. The observed shifts for the Q5–Q4–Q3 progression are -48 and -84 cm^{-1} , respectively. The second carbonyl mode progression starts with Q6 of the neutral species with a predicted frequency of 1689 cm^{-1} . This mode is a C2=O/C4=O out-of-phase stretch coupled to a slight N3H bend. The mode in the monoanion with an out-of-phase carbonyl stretching component is mode Q5 predicted at 1624 cm^{-1} . This mode is dominated by a C2=O stretching component coupled to a small N3H bending component. This corresponds to a predicted shift of -65 cm^{-1} for the neutral-to-monoanion

progression. Q7 of the dianion, predicted at a frequency of 1428 cm^{-1} , most closely correlates with Q5 of the monoanion in that it contains a large C2=O stretching component. The predicted shift in this case is -196 cm^{-1} . The observed shifts for the Q6–Q5–Q7 mode progression are -55 and -169 cm^{-1} , respectively. Details of these carbonyl mode correlations can be seen by comparing the first two rows of Table 6, which summarizes all predicted in-plane mode progressions in mode plot form.

Nine in-plane a' fundamentals are predicted in the 1200–1600 cm^{-1} region for each deuterated lumazine species examined. For the neutral species, these modes are Q7–Q15 with predicted frequencies of 1568, 1559, 1503, 1445, 1404, 1348, 1293, 1256, and 1236 cm^{-1} . The Raman spectrum of the neutral species (Figure 2C, pD 4.9) contains seven bands (Q9 and Q14 are not assigned in this spectrum). Seven bands are also seen in this energy region in the infrared data (Figure 2D, pD 5.0), with Q11 and Q14 unassigned in this case. For the monoanion, the nine fundamentals, Q6–Q14, have predicted frequencies of 1561, 1532, 1498, 1422, 1387, 1340, 1267, 1256, and 1205 cm^{-1} . All nine of the predicted fundamentals are seen in the Raman data (Figure 2C, pD 8.9), but only eight are assigned in the FTIR data (Figure 2D, pD 9.6) (Q10 is not assigned). In the dianion, the predicted fundamentals are Q4–Q6 and Q8–Q13 at the frequencies 1554, 1528, 1487, 1411, 1374, 1313, 1260, 1219, and 1193 cm^{-1} . Only seven of these modes are assigned in the Raman data (Figure 2C, pD 13.0) (Q4 and Q9 are not seen). Seven bands are also assigned in the FTIR data (Figure 2D, pD 13.4), with Q4 and Q10 not observed in this case. In general, mode correlations between the neutral and the monoanion forms of lumazine are much more difficult to make for the N-deuterated case than for the N-protonated case, especially in the 1200–1600 cm^{-1} region (see Table 6). Unlike the Q11 and Q12 modes in the neutral form of protonated lumazine that are composed entirely of NH and/or CH bending components, there are no modes of this nature in N-deuterated, neutral lumazine. A strong N1D bending component does not appear until the Q16–Q18 modes with predicted frequencies of 1188, 1155, and 1073 cm^{-1} . There is a small amount of N3D bend in the Q6 out-of-phase carbonyl mode but no other modes contain an N3D bending component until Q14 at 1256 cm^{-1} . For these modes and all modes to lower frequency, any ND bending component is coupled with a deformation of the lumazine heterocycle. In the A1/N3D monoanion, there is a small N3D bending component in mode Q5 at 1624 cm^{-1} , the out-of-phase carbonyl mode. The next mode with any appreciable N3D bending component is mode Q14 at 1205 cm^{-1} . As with the neutral species, any modes below this frequency possessing an N3D bending component also involve some distortion of the lumazine heterocycle. The predicted and observed shifts with ionization for this energy region agree very closely with no glaring differences in the neutral-to-monoanion shifts and only a few shifts worth noting on going from the monoanion to the dianion: Q9 to Q8 (predicted, -11 cm^{-1} ; observed, $+2$ cm^{-1}) and Q11 to Q10 (predicted, -27 cm^{-1} ; observed, $+1$ cm^{-1}). The Q11 to Q10 shift appears in the same region of the experimental spectra that caused some difficulty in assigning this region in the N-protonated forms of lumazine. The predicted Q11 to Q10 shift is -27 cm^{-1} , but the observed shift, as assigned in the experimental spectra, is $+1$ cm^{-1} . Applying the predicted monoanion-to-dianion shift of -27 cm^{-1} to the observed Q11 mode of the monoanion should put the Q10 band of the dianion at approximately 1297 cm^{-1} . In the Raman spectrum for the dianion (Figure 2C, pD 13.0), there is

one strong peak at 1325 cm^{-1} and another strong and much broader peak at 1299 cm^{-1} . In the FTIR data for the dianion (Figure 2D, pD 13.4), no 1325 cm^{-1} peak is seen but there is a very broad, strong peak at 1303 cm^{-1} . As in the N-protonated case, if the $1299/1303\text{ cm}^{-1}$ mode is reassigned to mode Q10, this mode shift discrepancy is cleared, but that leaves mode Q11 in the dianion unassigned. Mode Q12 in the monoanion, observed at 1292 cm^{-1} , is predicted to shift down only 7 cm^{-1} with loss of the deuterium at N3, so it may be that mode Q11 is just unresolved from the broad peak at 1299 cm^{-1} in the Raman spectrum and 1303 cm^{-1} in the FTIR spectrum.

In the $300\text{--}1200\text{ cm}^{-1}$ range, 14 a' fundamentals are predicted for the neutral form of lumazine with predicted frequencies of 1188, 1155, 1073, 1064, 900, 882, 762, 677, 620, 559, 484, 455, 363, and 300 cm^{-1} . Of these 14 modes, only nine can be assigned in the experimental spectra: Q18, Q24, Q27, Q37, and Q38 are not seen in either the Raman spectrum or the FTIR data. These modes are all predicted to have weak scattering Raman intensities as can be seen in the simulated neutral spectrum (Figure 2A, n/D spectrum). For the monoanion, 13 a' fundamentals are predicted at 1142, 1119, 1067, 964, 874, 784, 673, 642, 560, 509, 462, 373, and 313 cm^{-1} . Eleven of these 13 modes are assigned in the experimental spectra: only the two lowest energy modes, Q34 and Q35, are not seen in the Raman spectrum (Figure 2C, pD 8.9). For the dianion, 12 a' fundamental modes are expected at 1109, 1091, 993, 939, 778, 717, 665, 579, 510, 467, 396, and 315 cm^{-1} . From the experimental spectra, only eight of these modes can be assigned, with Q22, Q24, Q31, and Q32 not seen. The predicted and observed shifts on going from neutral to monoanion again agree quite favorably. The largest discrepancies are for the following progressions: Q28 to Q26 with a predicted shift of -4 cm^{-1} but an observed shift of $+7\text{ cm}^{-1}$, and Q31 to Q29 with a predicted shift of $+1\text{ cm}^{-1}$ but an observed shift of -3 cm^{-1} . For the monoanion to dianion progression, the largest discrepancy is for the Q16 to Q14 shift with a predicted shift of -10 cm^{-1} but an observed shift of $+12\text{ cm}^{-1}$. Overall, the average unsigned errors between predicted and observed shifts are 8.0 cm^{-1} for the neutral-to-monoanion progression and 12.4 cm^{-1} for the monoanion-to-dianion progression, comparable to the N-protonated lumazine analysis.

C. H/D Isotopic Shifts. As a further aid in normal mode assignments, predicted vibrational modes for the N-protonated and N-deuterated neutral lumazine species as well as the A1/N3H and A1/N3D monoanionic forms are correlated. These correlations are also made in the experimental spectra so that the predicted and observed H/D isotopic shifts can be compared directly. As is discussed further below, in several cases, the correlated normal modes do not agree exactly in all details, i.e., the motions are not identical.

C.1. Neutral Forms of Lumazine. The calculated and observed H/D isotopic shifts for neutral lumazine are listed in Table 8. The simulated and experimental Raman spectra complete with mode assignments and H/D isotopic shifts are shown in Figure 3A,B. Detailed descriptions of the normal modes for N-protonated, neutral lumazine are shown in Table 4/Column 1 and for N-deuterated, neutral lumazine in Table 6/Column 1. In the carbonyl stretching region for the neutral species of lumazine, the highest energy vibrational mode is the C2=O/C4=O in-phase stretch. In the N-protonated case, this mode is dominated by the C2=O stretching component coupled to a fairly strong N1H/N3H bending component. In the N-deuterated molecule, this mode has nearly identical contributions from the C2=O and C4=O stretching components but with no ap-

preciable ND coupling. With complete loss of ND coupling in the N-deuterated case, it may be expected that the H/D isotopic shift would be negligible for this mode. In each case, this mode corresponds to mode Q5 with predicted vibrational frequencies of 1725 cm^{-1} , a calculated H/D shift of 0 cm^{-1} . In the experimental spectra, Q5 is assigned as 1719 cm^{-1} in the N-protonated Raman spectrum (Figure 3B, pH 2.2) and as 1715 cm^{-1} in the N-deuterated Raman spectrum (Figure 3B, pD 4.9), an observed H/D shift of -4 cm^{-1} . The Q6 modes can be correlated due to their out-of-phase C2=O/C4=O stretching components. In the N-protonated case, this out-of-phase carbonyl stretch is dominated by the C4=O stretching component and there is again coupling to a strong N3H bend and, to a lesser extent, an N1H bend. Q6 in the N-deuterated case has equal contributions of C2=O and C4=O stretching components and retains an N3D bending component suggesting that there will be an appreciable H/D isotopic shift for this mode. Q6 has predicted vibrational frequencies of 1709 cm^{-1} for the N-protonated molecule and 1689 cm^{-1} for the N-deuterated molecule, a predicted H/D shift of -20 cm^{-1} . Consistent with this, the experimental frequencies are 1703 and 1677 cm^{-1} for the N-protonated and N-deuterated molecules, an observed H/D shift of -26 cm^{-1} . It is worth noting that the simulations of the Raman spectra in this energy region (Figure 3A) hint that the Q5 and Q6 modes for the N-protonated species may not be resolved, whereas in the N-deuterated case Q6 will shift away from Q5 far enough that it will resolve (or at least appear as a shoulder). In the experimental spectra for this region (Figure 3B), the Q5 and Q6 peaks in the pH 2.2 spectrum are not resolved (although this peak is fit best by two Lorentzian bands using the Peakfit program); by contrast, a shoulder is obvious in the pD 4.9 spectrum. Adding to the difficulties in resolving the bands in the pH 2.2 spectrum is the need to subtract a large solvent peak centered at approximately 1640 cm^{-1} . The Q5/Q6 region in the pD 4.9 spectrum is not influenced by solvent subtraction since this solvent band shifts down to approximately 1206 cm^{-1} in D_2O .

For the Q7–Q10 modes, the H/D isotopic shifts are predicted to be -6 , -2 , -7 , and -1 cm^{-1} . As in the case of the carbonyl stretching modes, each of these modes is predicted to have some NH bending component in the N-protonated molecule that is lost with deuterium substitution, resulting in only minor H/D shifts in these modes. The observed shifts for Q7–Q10 are -2 , -13 , -10 , and -8 cm^{-1} . For modes Q7–Q18, mode correlations between the N-protonated and the N-deuterated molecules is made difficult due to the differences in NH and CH bending component coupling with the motions of the lumazine heterocycle. The largest discrepancies are seen in the Q16 to Q15 H/D shift (predicted, -5 cm^{-1} ; observed, $+23\text{ cm}^{-1}$) and the Q18 to Q17 H/D shift (predicted, $+16\text{ cm}^{-1}$; observed, -21 cm^{-1}). For the remaining modes, mode correlations are much more straightforward in that the N-deuterated modes retain both the motions of the heterocycle and the bending components seen in the N-protonated molecule. Below 1100 cm^{-1} , the agreement between predicted and observed H/D shift is very good, best illustrated by the Q22 to Q22 and Q31 to Q29 H/D shifts. These modes are composed of fairly complex motions of the heterocycle coupled to both N1H and N3H bend/displacement type motions and thus are expected to show some isotope sensitivity. The Q22 to Q22 H/D shift is predicted to be -27 cm^{-1} and is observed at -28 cm^{-1} . The Q31 to Q29 H/D shift is predicted to be -35 cm^{-1} and is observed at -30 cm^{-1} . Overall, the average unsigned error between predicted and observed shifts with H/D substitution is 8.4 cm^{-1} .

C.2. Monoanionic Forms of Lumazine. Table 9 summarizes the calculated and observed H/D isotopic shifts for the monoanionic form of lumazine. Simulated and experimental Raman spectra including mode assignments and H/D shift magnitudes are shown in Figure 4A,B. Mode-by-mode comparisons can be made using the second columns of Table 4 and Table 6 for the N-protonated and N-deuterated molecules, respectively. In general, mode correlations for the monoanion are more straightforward than is the case for the neutral form of lumazine. Mode correlations are somewhat difficult in the Q12–Q19 region, but direct comparison of the predicted and observed H/D shifts results in an average unsigned error of 6.9 cm^{-1} with very good agreement on a mode-by-mode basis. In the monoanion, the carbonyl stretches for the N-deuterated molecule are not nearly as symmetric as is the case for neutral lumazine. The Q4 mode, predicted at a frequency of 1690 cm^{-1} and observed at 1667 cm^{-1} , is now dominated by the C4=O stretch with a small amount of in-phase C2=O stretch and no appreciable N3D bend. This mode correlates closely to Q4 of the N-protonated monoanion with a predicted frequency of 1699 cm^{-1} and an observed frequency of 1645 cm^{-1} , although there is a fairly strong N3H bending component in the N-protonated case (absent in N-deuterated). The predicted shift is -9 cm^{-1} , and the experimental shift is -16 cm^{-1} . The Q5 modes also correlate very closely, both dominated by C2=O stretching components coupled to an N3H(D) bending component. In the N-deuterated case, the Q5 mode also has a small out-of-phase C4=O stretching component. As seen with the neutral species, the carbonyl stretching mode that retains some ND bending component is predicted to have a larger H/D shift. For Q5, the predicted shift is -24 cm^{-1} and the observed shift is -23 cm^{-1} .

Very close correlations are evident for modes Q6–Q9 with predicted H/D shifts of -4 , -2 , -1 , and -2 cm^{-1} and observed shifts of 0 , -2 , $+1$, and -4 cm^{-1} . These modes are nearly isotope insensitive, with little or no bend/displacement at the N3 site, so it is not unexpected that H/D shifts are minimal. For modes Q10–Q19, mode correlations are not as obvious. The Q11 mode in the N-protonated monoanion is composed of strong C6H/C7H bending components coupled to a strong N3H bending component and has no corresponding mode in the N-deuterated monoanion. Q13, Q14, and Q19 in the N-protonated molecule and Q12, Q13, and Q19 in the N-deuterated molecule also have no corresponding modes. In general, the modes in this region that are correlated agree quite closely in magnitude and direction of shift, the largest discrepancy being the Q16 to Q16 shift: predicted shift of -5 cm^{-1} , observed shift of -22 cm^{-1} . The remaining modes in the monoanions correlate very closely and are composed of various distortions of the lumazine heterocycle. Those modes in the N-deuterated molecule that retain large N3D bending/displacement components again are predicted to have the largest H/D shifts in this region: for example, the Q20–Q22 correlation with a predicted shift of -57 cm^{-1} and an observed shift of -66 cm^{-1} . The Q27 to Q27 correlation is also notable with a predicted shift of -46 cm^{-1} and an observed shift of -28 cm^{-1} , although in this case the mode correlation is not quite as strong as that for modes Q20–Q22. The three lowest frequency modes assigned in the experimental spectra are clearly dominated by ring motions with only minor motions at the N3 position. Only minor H/D shifts are predicted for these correlations: Q30 to Q29, -3 cm^{-1} ; Q31 to Q31, -6 cm^{-1} ; and Q33 to Q32, -2 cm^{-1} , which agree very closely with the observed shifts of -1 , -3 , and $+1\text{ cm}^{-1}$, respectively.

Conclusions

In this study, we have assigned the $300\text{--}1750\text{ cm}^{-1}$ region of the vibrational spectra of (1H,3H)pteridine-2,4-dione (lumazine), recorded by FTIR and Raman spectroscopy in aqueous solution over the pH/pD range of 2–13, using first principles calculations of fundamental harmonic molecular vibrations. The aqueous environment was simulated by continuous reaction field methods while the existence of different lumazine protonation forms (neutral, anion, and dianion) was modeled using pteridine-2,4-dione (neutral lumazine), pteridine-2,4-dione A1 anion (lumazine anion), and pteridine-2,4-dione A1,A3-dianion (lumazine dianion). No imino-diol tautomeric forms of pteridine-dione were deemed necessary to complete the analysis. The vibrational spectra recorded over a wide pD range in deuterium oxide were interpreted with the help of the isotopically weighted calculated fundamental harmonic vibrations.

This analysis leads us to the following conclusions:

(i) Vibrational frequencies resulting from the SCM/DFT-B3LYP/4-31G method in a reaction field with a dielectric constant approximating bulk water ($\epsilon = 78.54$) scaled with a simple scale factor agree well with experiment for both the N-protonated and the N-deuterated lumazines. For the neutral and monoanionic forms of lumazine, the average unsigned error between predicted and observed vibrational frequencies was modest, ranging from 9.10 to 10.77 cm^{-1} . Agreement is not quite as good for the dianion with an average unsigned error of 16 cm^{-1} . This may have been a reflection of inadequacies in the reaction field method as applied to multiply charged molecules.

(ii) Vibrational mode shifts upon ionization predicted using the Kirkwood–Onsager dipole reaction field model agree fairly well with the shifts seen experimentally for both the N-protonated and the N-deuterated lumazines. Most pronounced are the observed red shifts in the carbonyl stretching region with progressive deprotonation for the N-protonated lumazines of -74 and -194 cm^{-1} (Q5–Q5–Q7) and -20 and -104 cm^{-1} (Q6–Q4–Q3) and for the N-deuterated lumazines of -48 and -84 cm^{-1} (Q5–Q4–Q3) and -55 and -169 cm^{-1} (Q6–Q5–Q7). Predicted and observed shifts for the neutral-to-monoanion mode progressions for both N-protonated and N-deuterated lumazines agree fairly well in both direction of shift and shift magnitude with average unsigned errors of 7 and 8 cm^{-1} for N-protonated and N-deuterated lumazines, respectively. The predicted and observed monoanion-to-dianion progressions do not compare as favorably, however, with some differences in direction of shift as well as magnitude for certain progressions. In the N-protonated case, the Q9–Q8, Q12–Q10, Q19–Q17, and Q31–Q28 and in the N-deuterated case, the Q9–Q8, Q11–Q10, Q12–Q11, and Q16–Q14 all show differences in direction of shift. Overall, the average unsigned error between predicted and observed shifts for the monoanion-to-dianion progression is approximately 12.5 cm^{-1} for both congeners.

(iii) Further correlations are made between ionization states of lumazine to compare the predicted and experimental H/D isotopic shifts. Again, overall agreement is quite good for both the neutral and the monoanion comparisons with average unsigned errors of 8.4 and 6.9 cm^{-1} , respectively. Only a few discrepancies arise in the neutral H/D shift comparisons: Q16/Q15, with a predicted shift of -5 cm^{-1} and an observed shift of $+23\text{ cm}^{-1}$, and Q18/Q17, with a predicted shift of $+16\text{ cm}^{-1}$ and an observed shift of -21 cm^{-1} . For the monoanion, predicted and observed H/D shifts are all in the same direction (except for some very minor shifts) but differ in magnitude in some cases. As anticipated, the largest downshifts are for those

modes that retain some amount of N1D and/or N3D bend/displacement after deuterium substitution. Notably, the Q6 out-of-phase carbonyl stretching modes in both the neutral and the monoanion that retain some N3D bend have predicted H/D shifts of -20 and -24 cm^{-1} , respectively, while the Q5 in-phase carbonyl stretching modes lose the ND bending component with predicted shifts of 0 and -9 cm^{-1} for the neutral and monoanion, respectively. Larger downshifts are seen for some of the lower energy modes that retain an ND bending component but which also include a displacement of the N atom of the labeled site. These include Q31/Q29 in the neutral molecule with predicted and observed H/D shifts of -35 and -30 cm^{-1} , respectively, and modes Q20/Q22 in the monoanion with predicted and observed H/D shifts of -57 and -66 cm^{-1} , respectively.

In summary, we point out the three objectives achieved by this study: first, we have obtained the midrange vibrational signature of the lumazine heterocycle, the Raman spectroscopic probe in our studies of the reaction mechanisms of molybdopterin oxotransferases;³ second, we have confirmed and extended our previous study of molecular vibrational and acid/base properties of a lumazine constituent ring, pyrimidine dione,⁷ and third, we have provided a basis for extending this type of study to the isoalloxazine ring, the heteroaromatic constituent of flavin enzyme cofactors. Most important, in both the experimental and the theoretical portions of the study is the inclusion of aqueous medium and explicit treatment of the different protonation forms that allowed us to obtain a vibrational and acid/base profile of this pteridine heterocycle, a pH sensitive spectroscopic probe and a versatile enzyme pseudo-substrate.

Acknowledgment. We thank Dr. J. O. Alben (The Ohio State University, Columbus, Ohio) for access to the FTIR instrument used in this study, Dr. W. A. Oertling (East Washington University, Cheney, Washington) for useful comments, and Dr. William L. Weaver (LaSalle University, Philadelphia, Pennsylvania) for preliminary contributions. This work was supported by the NIH through Grant GM 59953 and by The Ohio Supercomputer Center through Grant PAS0874.5.

Abbreviations

HF, Hartree–Fock; DFT, density functional theory; B3LYP, three parameter exchange functional of Becke combined with the Lee, Yang, and Parr correlation functional; SCM, spherical cavity model; SCIPCM, self-consistent isodensity polarizable continuum model; FTIR, Fourier transform infrared; SCRF, self-consistent reaction field; SQM, scaled quantum mechanical.

Supporting Information Available: Cartesian coordinates and the Z matrix for the optimized geometries of neutral lumazine, lumazine A1/N3H-monoanion, and lumazine A1,A3-dianion using the SCM/DFT-B3LYP/4-31G method. This material is available free of charge via the Internet at <http://pubs.acs.org>.

References and Notes

- (1) Davis, M. D.; Olson, J. S.; Palmer, G. J. *J. Biol. Chem.* **1982**, *257*, 14730.
- (2) Davis, M. D.; Olson, J. S.; Palmer, G. J. *J. Biol. Chem.* **1984**, *259*, 3526.
- (3) Kim, J. H.; Ryan, M. G.; Knaut, H.; Hille, R. *J. Biol. Chem.* **1996**, *271*, 6771.
- (4) Oertling, W. A.; Hille, R. *J. Biol. Chem.* **1990**, *265*, 17446.
- (5) Willis, L. J.; Loehr, T. M. *Biochemistry* **1984**, *24*, 2768.
- (6) Using excitation outside of the 290–550 nm region avoids interference due to vibrational modes of the protein matrix and the other chromophores of xanthine oxidase, two Fe/S clusters of the spinach ferredoxin variety and one flavin adenine dinucleotide per enzyme subunit.
- (7) Ilich, P.; Hemann, C. F.; Hille, R. *J. Phys. Chem. B* **1997**, *101*, 10923.
- (8) Barnes, A. J.; Stuckey, M. A.; Le Gall, L. *Spectrochim. Acta* **1984**, *40A*, 419.
- (9) Szczesniak, M.; Nowak, M. J.; Rostkowska, H.; Szczepaniak, K.; Person, W. B.; Shugar, D. *J. Am. Chem. Soc.* **1983**, *105*, 5969.
- (10) Maltese, M.; Passerini, S.; Nunziante-Cesaro, S.; Dobos; Harsanyi, L. *J. Mol. Struct.* **1984**, *116*, 49.
- (11) Graindourze, M.; Smets, J.; Zeegers-Huyskens, T.; Maes, G. *J. Mol. Struct.* **1990**, *222*, 345.
- (12) Les, A.; Adamowicz, L.; Nowak, M. J.; Lapinski, L. *Spectrochim. Acta* **1992**, *48A*, 1385.
- (13) Ivanov, A. Yu.; Plokhhotnichenko, A. M.; Radchenko, E. D.; Sheina, G. G.; Blagoi, Yu. P. *J. Mol. Struct.* **1995**, *372*, 91.
- (14) Kirkwood, J. G. *J. Chem. Phys.* **1934**, *2*, 351.
- (15) Onsager, L. *J. Am. Chem. Soc.* **1936**, *58*, 1486.
- (16) Beens, H.; Weller, A. *Chem. Phys. Lett.* **1969**, *3*, 666.
- (17) Wong, M. W.; Wiberg, K. B. *J. Chem. Phys.* **1991**, *95*, 8991.
- (18) Foresman, J. B.; Keith, T. A.; Wiberg, K. B.; Snoonian, J.; Frisch, M. J. *J. Phys. Chem.* **1996**, *100*, 16098.
- (19) Wiberg, K. B.; Rablen, P. R.; Rush, D. J.; Keith, T. A. *J. Am. Chem. Soc.* **1995**, *117*, 4261 and references therein.
- (20) Frisch, M. J.; Frisch, A.; Foresman, J. B. *Gaussian 94 User's Reference*; Gaussian, Inc.: Pittsburgh, PA, 1994–1995; pp 144–146.
- (21) Albert, A.; Brown, D. J.; Cheeseman, G. *J. Chem. Soc.* **1951**, 474.
- (22) Gutfreund, H. *Enzymes: Physical Principles*; John Wiley and Sons: New York, 1977; p 173.
- (23) Kohn, W.; Becke, A. D.; Parr, R. G. *J. Phys. Chem.* **1996**, *100*, 12974.
- (24) Andzelm, J.; Wimmer, E. *J. Phys. Chem.* **1992**, *96*, 1280.
- (25) Johnson, B. G.; Gill, P. M. W.; Pople, J. A. *J. Phys. Chem.* **1993**, *98*, 5612.
- (26) Becke, A. D. *J. Chem. Phys.* **1993**, *98*, 5648.
- (27) Becke, A. D. *Phys. Rev.* **1988**, *A38*, 3098.
- (28) Lee, C.; Yang, W.; Parr, R. G. *Phys. Rev.* **1988**, *37B*, 785.
- (29) Clark, T.; Chandrasekhar, J.; Spitznagel, G. W.; Schleyer, P. v R. *J. Comput. Chem.* **1983**, *4*, 293.
- (30) Ditchfield, R.; Hehre, W. J.; Pople, J. A. *J. Chem. Phys.* **1971**, *54*, 724.
- (31) Frisch, M. J.; Trucks, G. W.; Schlegel, H. B.; Gill, P. M. W.; Johnson, B. G.; Robb, M. A.; Cheeseman, J. R.; Keith, T.; Petersson, G. A.; Montgomery, J. A.; Raghavachari, K.; Al-Laham, M. A.; Zakrzewski, V. G.; Ortiz, J. V.; Foresman, J. B.; Cioslowski, J.; Stefanov, B. B.; Nanayakkara, A.; Challacombe, M.; Peng, C. Y.; Ayala, P. Y.; Chen, W.; Wong, M. W.; Andres, J. L.; Replogle, E. S.; Gomperts, R.; Martin, R. L.; Fox, D. J.; Binkley, J. S.; Defrees, D. J.; Baker, J.; Stewart, J. P.; Head-Gordon, M.; Gonzalez, C.; Pople, J. A. *Gaussian 94*, revision C.3; Gaussian, Inc.: Pittsburgh, PA, 1995.
- (32) Dewar, M. J. S.; Zoebisch, E. G.; Healy, E. F.; Stewart, J. J. P. *J. Am. Chem. Soc.* **1985**, *107*, 3902.
- (33) Dewar, M. J. S.; Thiel, W. *J. Am. Chem. Soc.* **1977**, *99*, 4899.
- (34) (a) Stewart, J. J. P. *J. Comput. Chem.* **1989**, *10*, 209. (b) Stewart, J. J. P. *J. Comput. Chem.* **1989**, *10*, 221.
- (35) Kurinovich, M. A.; Lee, J. K. *J. Am. Chem. Soc.* **2002**, *122*, 6258.
- (36) Michaud, A. L.; Herrick, J. A.; Duplain, J. E.; Manson, J. L.; Hemann, C.; Ilich, P.; Donohoe, R. J.; Hille, R.; Oertling, W. A. *Biospectroscopy* **1998**, *4*, 235.
- (37) Schmidt, M. W.; Baldridge, K. K.; Boatz, J. A.; Elbert, S. T.; Gordon, M. S.; Jensen, J. H.; Koseki, S.; Matsunaga, N.; Nguyen, K. A.; Su, S. J.; Windus, T. L.; Dupuis, M.; Montgomery, J. A. *J. Comput. Chem.* **1993**, *14*, 1347.
- (38) Xidos, J. D.; Li, J.; Zhu, T.; Hawkins, G. D.; Chuang, Y.-Y.; Fast, P. L.; Liotard, D. A.; Rinaldi, D.; Cramer, C. J.; Truhlar, D. G. *GAMESOL*, version 3.0; University of Minnesota: Minneapolis, 2001, based on GAMESS (ref 37).
- (39) Brown, D. J. In *Fused Pyrimidines. Part Three, Pteridines*; Taylor, E. C., Ed.; John Wiley & Sons: New York, 1988.
- (40) Rauhut, G.; Pulay, P. *J. Phys. Chem.* **1995**, *99*, 3093.
- (41) Martin, J. M. L.; El-Yazal, J.; Francois, J.-P. *J. Phys. Chem.* **1996**, *100*, 15358.
- (42) Hurst, J. K.; Wormell, P.; Bacskay, G. B.; Lacey, A. R. *J. Phys. Chem. A* **2000**, *104*, 7386.
- (43) Albert, A. *Biochem. J.* **1953**, *54*, 646.